Earth and Planetary Science Letters 385 (2014) 1–11

Contents lists available at ScienceDirect

Earth and Planetary Science Letters

www.elsevier.com/locate/epsl

Structure of the crust and the lithosphere beneath the southern Puna plateau from teleseismic receiver functions

B. Heit [a,*], M. Bianchi [a,h], X. Yuan [a], S.M. Kay [b], E. Sandvol [c], P. Kumar [a,d], R. Kind [a,e], R.N. Alonso [f], L.D. Brown [b], D. Comte [g]

[a] Deutsches GeoForschungsZentrum GFZ, Telegrafenberg, 14473 Potsdam, Germany
[b] Cornell University, EAS, Snee Hall, Ithaca, NY 14850, United States
[c] Department of Geological Sciences, University of Missouri, Columbia, MO 65211, United States
[d] NGRI, Hyderabad, India
[e] Freie Universität Berlin, Maltesserstr. 74-100, 12227 Berlin, Germany
[f] Universidad Nacional de Salta, Buenos Aires 177, 4400 Salta, Argentina
[g] Departamento de Geofisica, Universidad de Chile, Santiago, Chile
[h] Institute of Astronomy, Geophysics and Atmospheric Sciences, University of São Paulo, Rua do Matão 1226, 05508-090 São Paulo, SP, Brazil

ARTICLE INFO

Article history:
Received 5 July 2013
Received in revised form 6 October 2013
Accepted 9 October 2013
Available online 1 November 2013
Editor: P. Shearer

Keywords:
Central Andes
Puna plateau
teleseismic receiver functions
crustal thickness
lithosphere–asthenosphere boundary

ABSTRACT

We present a teleseismic P and S receiver function study using data from a temporary passive-source seismic array in the southernmost Puna plateau and adjacent regions. The P receiver function images show the distribution of crustal thickness and V_p/V_s ratio for this area. Over much of the southern Puna plateau, the crustal thickness is 50–55 km, whereas to the west a thicker crust (~60 to 75 km) is observed beneath much of the Andean volcanic arc region. From the Puna southward, there is little obvious change in the crustal thickness across the border of the plateau (south of 28°S). The crust is seen to progressively thin towards the east in the Pampean Ranges where it is 35–40 km thick. The southern Puna plateau is characterized overall by a low crustal V_p/V_s ratio (less than 1.70), implying a felsic crustal composition. An anomalously high V_p/V_s ratio of 1.87 is observed beneath the Cerro Galan volcanic center, in the region where a prominent crustal low-velocity zone identified below ~10 km depth probably extends into the lower crust. The crustal thickness determined under the Cerro Galan area (59 km) is close to that of the rest of the southern Puna. The prominent high V_p/V_s ratio and low-velocity zone beneath the Galan region implies the presence of a zone of partial melt or a magma chamber is consistent with hypothesis calling for lithospheric delamination beneath the Galan caldera. A widespread crustal low-velocity layer observed beneath much of the southern Puna, correlates well with crustal low-velocity anomalies observed by teleseismic tomography. The lithosphere–asthenosphere boundary beneath the array can be clearly observed by both P and S receiver functions at depths of 70–90 km in agreement with previous studies suggesting a thin lithosphere beneath the high elevated plateau. The mantle transition zone discontinuities appear at expected depths.

1. Introduction

The Altiplano–Puna region (marked as Puna in Fig. 1) in the Central Andes is a high elevated plateau that was formed in a subduction regime, which is flanked to the north and south by segments of flat subduction. The inherited plateau geological history, uplift, shortening and magmatism have been studied over the last decades (e.g., Cahill and Isacks, 1992; Allmendinger et al., 1997; Oncken et al., 2003; Kay and Coira, 2009 and references therein) and distinct differences have been recognized between the Altiplano to the north and the Puna to the south. In this paper we focus on the crustal and lithospheric structure beneath the southern end of the Puna plateau, until recently a geophysically poorly studied area. In a new study, Bianchi et al. (2013) gave an account of available geophysical information on the southern Puna plateau based on a number of studies, which began with the pioneering Magnetotelluric experiments of Febrer et al. (1982). To the south of 30°S, a number of seismic studies provide clues to the Moho, the lithosphere and the seismicity in the area located above the Chilean flat-slab region (e.g. Fromm et al., 2004; Alvarado et al. 2005, 2007; Gilbert et al., 2006; Gans et al., 2011; Porter et al., 2012, Ward et al., 2013).

The main features distinguishing the southern Puna plateau from the northern Puna and the Altiplano are: (a) a thinner continental lithosphere (Whitman et al., 1992; Heit et al., 2007), (b) the

* Corresponding author.
E-mail address: heit@gfz-potsdam.de (B. Heit).

0012-821X/$ – see front matter
http://dx.doi.org/10.1016/j.epsl.2013.10.017

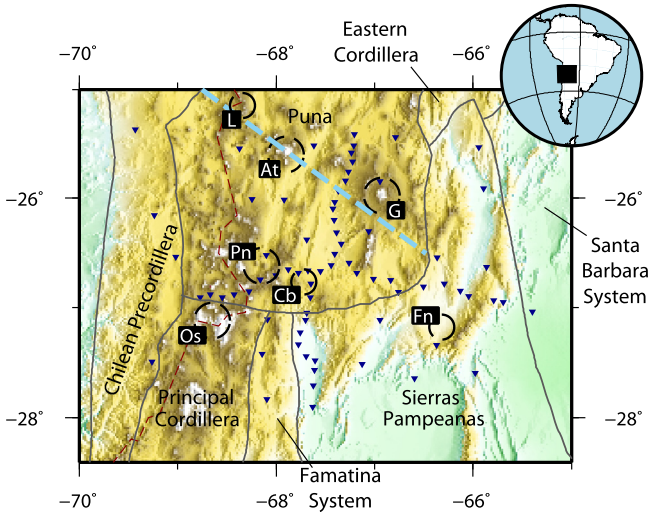

Fig. 1. Map showing the distribution of stations (blue inverted triangles) and the tectonic units (grey lines) in the southern Puna. Red triangles denote volcanoes. The red dashed line is the Chile/Argentina border. Volcanic centers inside the array are marked with black circles; At: Antofalla; G: Cerro Galan Caldera; Pn: Peinado; Cb: Cerro Blanco Caldera; Os: Ojos del Salado; Fn: Farallon Negro. The blue dashed line is the trace of the Archibarca lineament that runs from the northwest at the position of the Lastarria volcano (marked as L) to the southeast in the southern Puna plateau. (For interpretation of the references to color in this figure legend, the reader is referred to the web version of this article.)

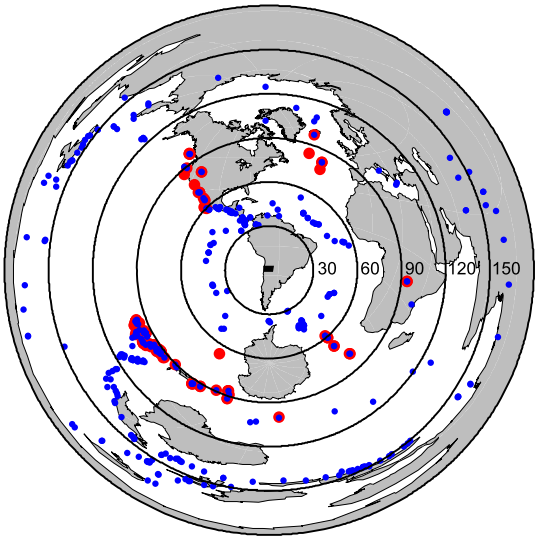

Fig. 2. Map of teleseismic earthquakes used in this study. Blue circles denote epicenters in a distance range of 30°–180° used for P and PP phases. Red circles denote earthquakes at epicentral distances between 60° and 115° used for S and SKS phases. Black concentric circles marked as reference for epicentral distances every 30°. (For interpretation of the references to color in this figure legend, the reader is referred to the web version of this article.)

subducting Nazca plate begins to shallow to the south (e.g., Cahill and Isacks, 1992; Mulcahy et al., submitted for publication) and (c) a distinctive sedimentary, magmatic and structural history (e.g. Coira et al., 1993; Kay et al., 1994, 1999; Allmendinger et al., 1997; Kay and Coira, 2009). Tectonically, the southern Puna has experienced less shortening than the Altiplano and the deformation is mainly concentrated in the eastern border of the plateau in the Eastern Cordillera and the Pampean Ranges (e.g., Kley and Monaldi, 1998; Kley et al., 1999). The large ignimbritic deposits in the area of the Cerro Galan caldera are suggested to be a consequence of piecemeal delamination of lithospheric material in the southern Puna (Kay and Kay, 1993; Kay et al. 1994, 2011).

Previous geophysical studies revealed low velocities in the crust and asthenosphere beneath the southern Puna plateau, suggesting higher temperatures than under the northern Puna and the Altiplano (e.g. Isacks, 1988; Whitman et al., 1992, 1996; Heit, 2005; Heit et al., 2007, 2008; Woelbern et al., 2009; Bianchi et al., 2013). The maximum crustal thickness along a profile at 25.5°S latitude obtained from a receiver function image, was nearly 60 km and the tomographic images show low-velocity anomalies in the crust that lessen into the mantle, consistent with asthenospheric material just below the Moho (Heit, 2005; Woelbern et al., 2009).

Here we apply the receiver function method to the teleseismic data recorded by the southern Puna passive-source seismic array, consisting of 74 stations (Fig. 1). In the analysis, we examine crustal thicknesses and intra-crustal layers with P receiver functions (PRF) and the lithosphere–asthenosphere boundary with S receiver functions (SRF).

2. Data and methodology

The seismic stations of the southern Puna array (Fig. 1) were distributed in two orthogonal profiles with a center at approximately 26.5°S and 67.5°W, which were surrounded by a sparser 2D array covering an area of approximately 300 × 300 km. For details concerning the station spacing and instrumentation see Bianchi et al. (2013). The data are archived at IRIS and GEOFON data centers.

We performed the teleseismic PRF receiver function analyses using events from the PDE catalog for which teleseismic P and PP phases were recorded at epicentral distances between 30° and 180° and for which magnitudes (mb) were greater than 5.5. For the SRF receiver function (including S and SKS phases), the epicentral distances were between 60° and 115° and magnitudes were greater than 5.5. The events used are shown in Fig. 2. The PRF computation was performed following the approach described by Yuan et al. (1997), whereas the SRF computation was performed using the approach by Kumar et al. (2006) and Yuan et al. (2006).

Seismograms with high signal/noise ratio have been visually inspected and manually selected for calculation of the P and S receiver functions. They were rotated, deconvolved and move out corrected for a constant reference slowness of 6.4 s/deg. The PRF were then divided into boxes according to piercing point locations at 60 km depth and stacked inside the boxed regions shown in Figs. 3 and 4 to enhance the signal-to-noise ratios of single traces (Dueker and Sheehan, 1997). We maximized the signal-to-noise ratios and homogenized the resolution based on the distribution of the stations in the array. We also enhanced coherent signals, like the Moho phase, at the same time that we suppressed random noise effects by stacking single traces from different events around stations in 0.5 × 0.5 deg boxes. Along the north–south and east–west profiles where the station spacing is about 10 km (Fig. 3), the boxes overlap by 0.1 deg. For the stations surrounding the two orthogonal profiles, similar sized boxes (i.e. 0.5 × 0.5 deg) do not overlap due to the larger station spacing (i.e. 50 km to 100 km; Fig. 4). In most cases, the Moho converted phase can be clearly recognized providing reliable estimates of the Moho depth.

Using the information provided by different crustal reverberations also known as Moho multiples, we estimated the Moho depth and the crustal V_p/V_s ratio following the H–K stacking approach (Zhu and Kanamori, 2000). The H–K stacks are done by boxes along the profiles north–south and west–east and by station piercing points elsewhere in the array since there are no overlaps where the station spacing is big. Some examples are presented in Fig. 5. Within each group a grid search is performed for estimates of Moho depth and crustal V_p/V_s ratio as indicated by the position of the maximum. The resulting V_p/V_s map shown in Fig. 6 illustrates the V_p/V_s variations in the region. Using the Moho depth values obtained by the H–K stacking method, we obtained a Moho depth map for the region (Fig. 7).